Passive Radar Detection of Aerial Targets

EROL ALI
ANDREAS ÖRSTADIUS
MASTER´S THESIS
DEPARTMENT OF ELECTRICAL AND INFORMATION TECHNOLOGY
FACULTY OF ENGINEERING | LTH | LUND UNIVERSITY

Passive Radar Detection of Aerial Targets

Erol Ali
gel10eal@student.lu.se

Andreas Örstadius
ark06aor@student.lu.se

May 23, 2017

Abstract

 The purpose of this thesis is to construct a passive bistatic radar system using two USRP N200 software defined radios and two ordinary TV-antennas. Several auxiliary components were used in order to align and calibrate the devices including an octoclock CDA-2990, switch and signal generator. Several tests were made to verify that the sampling started simultaneously and that no significant phase shift existed between the devices due to the use of different local oscillators. The system is implemented in C++ and the signal processing is done in MATLAB making use of the ambiguity function. Measurements were conducted on a commercial aircraft landing at Linköping airport and on an UAV. The results from these measurements show their bistatic range and bistatic velocity in 2D color plots.

Acknowledgements

Contents

Nomenclature

ADC - Analog-to-Digital Converter

ADS-B - Automatic Dependent Surveillance-Broadcast

DC - Direct Current

DDC - Digital Down-Converter

DSP - Digital Signal Processing

DVB-T - Digital Video Broadcasting-Terrestrial

EDA - Europan Defense Agency

FFT - Fast Fourier Transform

FOI - Totalförsvarets Forskningsinstitut

FPGA - Field-Programmable Gate Array

GNSS - Global Navigation Satellite System

GPS - Global Positioning System

LO - Local Oscillator

MIMO - Multiple-Input and Multiple-Output

NATO - North Atlantic Treaty Organization

NIC - Network Interface Controller

OFDM - Orthogonal Division Frequency Multiplexing

PBR - Passive Bistatic Radar

PfP - Partnership for Peace

PLL - Phase-Locked Loop

PPS - Pulse-per-second

PSK - Phase-Shift Keying

QAM - Quadrature Amplitude Modulation

Radar - Radio Detection And Ranging

RCS - Radar Cross Section

RMS - Root Mean Square

SDR - Software Defined Radio

SFDR - Spurious-Free Dynamic Range

SNR - Signal-to-Noise Ratio

SSD - Solid State Disk

TCP/IP - Transmission Control Protocol/Internet Protocol

UAV - Unmanned Aerial Vehicle

UHD - USRP Hardware Driver

UHF - Ultra High Frequency

USRP - Universal Software Radio Peripheral

Chapter 1

Introduction

This Master's thesis work at LTH was carried out in Linköping at *Totalförsvarets Forskningsinstitut*, FOI . FOI is a Swedish research institute in the areas of defense and national security. This project concerns the construction of a passive bistatic radar (PBR) system, verification of the system and includes an analyze of the collected data.

1.1   Background

Radar systems make use of radio waves in the electromagnetic spectrum to detect and localize objects by noting the time difference between the sent and received wave. The frequencies used are usually between 5 MHz and 95 GHz, although frequencies outside this span may very well be used with success [28]. The characteristics of the radar depend on what frequency that is used, *e.g.* low frequencies may detect targets at a longer range while a high frequency allows for a more accurate determination of range and location due to a wider bandwidth.

The technology was developed during the pre-World War II era and it was refined and used intensively after the outbreak of the war, then mainly as an aid in air defense and air combat. After the war had ended, the possibility to measure the Doppler shift in radar applications was starting to be widely explored. This allowed the radars to determine a target's velocity relative to the radar and thus be able to separate a target from the stationary clutter [28]. Radars at the beginning of the war were limited to only being able to detect a target's position and the tracking of the targets had to be done manually [21]. Although, many aspects such as antenna construction, range, available frequencies, accuracy and resolution were refined during the following years.

Radar is today used in several military applications, but has also significance in many civilian fields. These include among other air-, terrestrial- and marine traffic control, radar astronomy, geological measurements, both small and large scale surveillance systems, meteorological predictions and many more. One major contribution for the advancement of

radar systems since the World War II-era is the development of signal processing techniques which allows for a higher accuracy and resolution [26].

A radar system can have a variety of different configurations, of which some includes; a single antenna, multiple antennas, monostatic geometry, bistatic geometry, continuous wave and pulsed radar. With a monostatic geometry the antennas of the system are collocated, whereas in a bistatic geometry the transmitter and receiver are separated by a distance comparable to the distance of potential targets. The configuration that is used for this thesis is a bistatic geometry using a fixed Digital Video Broadcasting-Terrestrial (DVB-T) transmitter as a transmitter of opportunity and ordinary TV-antennas and the software defined radio (SDR), Universal Software Radio Peripheral (USRP) N200 at the receiving end. Since the transmitting antenna is a non-cooperative source the system is called a passive bistatic radar system. Because of the utilization of the already existing ambient spectrum this setup offers several beneficial effects, but also comes with an increased complexity to realize. Included among the advantages are, as mentioned in [27]:

- Low cost because of the utilization of an already existing transmitting antenna.

- High mobility and easy to relocate.

- Very fast update of target position.

- Possible ability to detect stealth targets that are otherwise undetectable.

- Virtually undetectable because of no transmitting antenna at receiving location.

1.1.1 Previous work

FOI in Linköping has previous experience of passive radar systems. Methods have been developed and tested for using this technique on aircrafts to detect the ground-level topography.

Another Master's thesis has been done at the Norwegian University of Science and Technology carried out at FFI (Forsvarets forskningsinstitutt) [3]. The report concerns passive radar which is processed with the Ambiguity Function with an analysis of range and Doppler walk.

A doctoral dissertation has been done at University College London [2]. Although it concerns airborne passive radar it contains conceptual and theoretical descriptions also applicable on ground based passive radar.

Passive radar is a well known subject for which many studies exist, but studies concerning the construction and analysis of a PBR system with a general SDR are scarce. General SDRs are flexible with respect to wide range frequency tuning and can maintain a high bandwidth if Ethernet connectivity is available.

1.1.2 Aims and Challenges

The aim for this thesis is to construct a PBR system that accurately shows the range and Doppler frequency of aerial targets using two SDRs. The system should also be modifiable as to include additional devices if desired. Also, the receiving frequency should be tunable

over a wide range so that many different signal sources can be chosen in different frequency bands.

The main challenges will be to configure and setup a functioning receiver system and to perform the digital signal processing (DSP) on the collected data. Since two receivers will be used, another challenge is to make sure that they are synchronized internally with respect to each other, including that they start sampling at the same time.

There already exist ample software variations for the hardware that will be used. Here the challenge will be to modify these to suit the strict requirements on the receiving mechanisms. Otherwise, the result from the DSP processing may be erroneous.

The sampled data needs to be transferred to the processing computer which give rise to other challenges, such as the sampling frequency and bandwidth of the local network. The reconstruction of the signal will be more accurate by sampling the signal with a higher rate. The consequence will be an increase of data that needs to be transferred from the receiving device to the host computer occupying more bandwidth on the network. Furthermore, the Ethernet cable and Network Interface Controller (NIC) sets the limit on the amount of data that can be received per second. If the data rate exceeds this limit, packages will be lost. During the processing it is crucial that the samples have been received in a continuous stream.

To validate the PBR system an Automatic Dependent Surveillance - Broadcast (ADS-B) receiver will be incorporated in the system as "ground truth". This gives rise to more challenges due to the increase of system components that need to be considered and the additional data to be processed.

1.2   FOI

FOI is the Swedish defense and research agency and an assignment-based authority under the Ministry of Defense. The Armed Forces and the Swedish Defense Material Administration are their main customers but they also accept assignments from civil authorities and industry. FOI also has international customers and cooperation partners among foreign authorities. They cooperate in EU-financed projects with European Defense Agency (EDA) and the Partnership for Peace (PfP), program by North Atlantic Treaty Organization (NATO) .

The employees at FOI have various areas of expertise such as science, law, philosophy and economy. For this reason, FOI can carry out studies in security policy and analyses of various types of threats. Building a prototype of a technological system is another example of typical assignments. The prototype can then be evaluated in the field for further analyses. The whole chain from an idea for a study to practical tests and later analyses of the system is conducted at FOI when they accept an assignment.

Other, more specific examples of activities at FOI follows below [12]:

- How to detect explosive substances.

- Extract underwater signatures of ships in brackish and coastal waters.

- Design models of turbulent flows, such as underwater currents or air currents around aircraft.

- Constructing models and tools for society to adapt to the consequences of climate change.

- Continuing research on IT security and human system interaction.

1.3   Thesis Outline

- **Chapter 1. Introduction**

  The first chapter in this thesis gives a general description of the PBR along with a mention of previous studies in this area. It also discusses the main goal of this study and the primary challenges.

- **Chapter 2. Theory**

  The second chapter accounts for the basic theory that concerns a PBR system and typical effects that occurs due to the bistatic geometry. As well as describing the signal processing used during this thesis.

- **Chapter 3. System architecture**

  In this chapter the requirements on the system will be discussed followed by a description of each component used in the system, including a brief characterization of the USRP N200. It ends by showing the final experimental setup of the PBR system.

- **Chapter 4. Software implementation**

  Chapter 4 describes the implementation of the software. There is a detailed description of each program in both C++ and MATLAB with associated flowcharts. Prior to these sections will be a short summary of an initial MATLAB attempt to operate the system.

- **Chapter 5. System verification**

  In this chapter the verification of the system is presented. Describing the measures taken in order to synchronize the system and how the phase offset were dealt with.

- **Chapter 6. Simulation**

  This chapter describes the simulation process and the results obtained. By comparing the results with the theoretical outcome the simulation were used to verify that the signal processing code were conducted properly.

- **Chapter 7. Live measurements**

  Here the results from live measurements will be presented along with an explanation of how the results were obtained. A method that were intended to validate the system with the use of the ADS-B receiver will be presented. For reasons explained in the chapter this method did not work due to certain circumstances for this thesis.

- **Chapter 8. Overall conclusions**

  The final chapter summarizes the achievements of this thesis as well as discusses certain limitations and improvements. Some examples of different applications will conclude the report.

Included in the appendix is a manual of how to operate the program to perform measurements.

Chapter 2
Theory

The content of this chapter describes some of the effects arising due to the bistatic geometry, mainly the effects on the velocity component and radar cross section (RCS) . The geometry will be explained as well as some restrictions on the line of sight, including an estimate of the duration a target remains inside the antenna lobe. The properties of the DVB-T signal will be explained, showing why this signal is desired in a PBR system. The last section will account for the signal processing scheme using the ambiguity function that is used in this project as well as address the phenomenon of range and Doppler walk.

2.1 Bistatic geometry

In a PBR system the transmitting antenna and the receiving antenna are not collocated. Due to the separation, the receiving antenna is virtually undetectable, and by using a transmitter of opportunity it is impossible for a target to know if it has been detected [7]. The location of the antennas gives rise to two focal points in an ellipse. For every point on the ellipse, the sum of the distances to the focal points are constant.

The bistatic geometry is illustrated in figure 2.1 where the transmitting and receiving antenna is referred to as T_x and R_x respectively. L is known as the baseline, *i.e.* the distance between the transmitter and receiver. R_{tx} and R_{rx} is the distance between the transmitter and the receiver to the target, respectively.

In this project, two collocated receiving antennas will be used to independently receive signals. One of the antennas will be directed to receive the direct path signal from the transmitter, usually referred to as the reference antenna. The second antenna will be directed to receive the reflected time-delayed signal from both moving and stationary targets, usually referred to as the surveillance antenna. This antenna will also receive time-delayed signals from stationary targets. The difference in time between the two received signals, the bistatic delay τ, is due to the longer distance traveled for the reflected signal. This delay relates to the distance parameters in the bistatic geometry and the speed of light, c,

according to (2.1). Accordingly, the bistatic range is $\tau \cdot c$.

$$\tau = \frac{R_{tx} + R_{rx} - L}{c} \tag{2.1}$$

Equation (2.1) can be expressed as in (2.2) to obtain the sum of the distances to the two antennas.

$$R_{tx} + R_{rx} = \tau \cdot c + L \tag{2.2}$$

In (2.2), τ is estimated with the cross-correlation function and L can be measured by coordinates given by *e.g.* Google maps. For the most basic PBR system using only two antennas (reference and surveillance), as is the case for this thesis, the bistatic range and $R_{tx}+R_{rx}$ are the only distances that can be discerned. Consequently, it is not possible to determine the distance from the target to the receiving location.
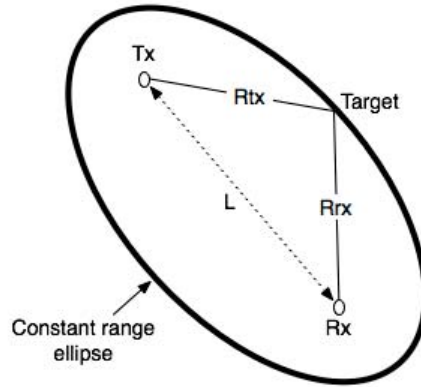
Figure 2.1: *The bistatic geometry of a PBR system*[15].

As previously mentioned the total distance $R_{tx} + R_{rx}$ is constant for every point on an ellipse as shown in figure 2.1. With the system used in this thesis it is thus impossible to know where on the ellipse a detected target is without having a priori knowledge of the direction of the surveillance antenna. Even with this knowledge the target still has an arbitrary position along the ellipse within the surveillance antennas beam width. Thus, in order to have a PBR system with high resolution and wide coverage a multiple-input and multiple-output (MIMO) configuration is required where the surveillance antennas has overlapping beams.

2.1.1 Bistatic velocity and Doppler shift

For a monostatic radar, where the transmitter and receiver are collocated, the Doppler frequency depends on the direction of the target. If the target travels straight towards or

straight away from the radar the measured Doppler frequency corresponds to the targets full velocity. If the target travels parallel to the radar the Doppler shift will be zero and the target will be discerned as a stationary target. The velocity component approximately corresponds to the Doppler frequency according to 2.3,

$$v = \frac{f_d c}{2 f_c} \tag{2.3}$$

where f_d is the Doppler shift, c the speed of light and f_c the carrier frequency. This is only the radial speed, the targets true velocity is obtained by dividing by $\cos(\delta)$ where δ is the angle between the radar and the direction of the target.

The expression for the velocity component, or the bistatic velocity, in the bistatic case is similar to the monostatic but also accounts for the fact that the antennas are not collocated. In this case the bistatic velocity is given by (2.4), where β, the bistatic angle, is the angle between R_{tx} and R_{rx}.

$$v_B = \frac{f_d c}{2 \cos(\beta/2) f_c} \tag{2.4}$$

As in the monostatic case, the true velocity is obtained by dividing with $\cos(\delta)$. Although, for a bistatic configuration, δ is the angle between the targets trajectory and the bisector of the R_{tx} and R_{rx} corner.

Furthermore, the Doppler shift can be expressed as the change in total traveled distance of the transmitted signal during a certain time interval as in (2.5) [6] [18].

$$f_d = \frac{d(R_{tx} + R_{rx})}{dt} \frac{f_c}{c} \tag{2.5}$$

2.1.2 Bistatic radar cross section

Normally, the radar cross section of a target is lower in a bistatic configuration than if it would have been in a monostatic configuration. There are however instances at certain bistatic angles where the bistatic RCS is greatly enhanced and even surpasses the monostatic RCS [6].

When the target is located close to the baseline, *i.e.* β is close to 180°, the scattering effects from the target are greatly enhanced, a phenomenon known as forward scattering [1]. In this configuration the bistatic radar is thus consequently called a forward scattering radar. This effect occurs because the target partly blocks the transmitted wave and acts as a black body which yields a hole in the wavefront. Instead there only exists a scattered field, also known as a shadow field, that only depends on the silhouette of the target [4].

A consequence of this is that targets designed by stealth technologies are detectable in this configuration. Aircrafts or cruise missiles designed with stealth technology have a shape that deflects incoming radar signals in other directions for certain aspect angles and utilizes a radar absorbing material [32]. Since only the silhouette affects the RCS in a forward scattering configuration these countermeasures does not affect the detectability [1].

Although the RCS has a peak in a forward scattering radar, the Doppler shift will be extremely small. Solving for f_d in (2.4) shows that the Doppler shift will be close to zero as β approaches 180°.

Although a monostatic radar normally has a larger RCS from a target than the bistatic counterpart, an inherent enhancer of the RCS are the frequencies used when using commercial transmitters of opportunity. The wavelengths used in a PBR can be in the decimeter to meter range depending on the source, *i.e.* in some cases the wavelength is on the same order of magnitude as the target. When this is the case, the transmitted wave and the target resonates and increases the RCS of the target. The RCS induced by resonance is also not dependent on the shape of the target, further increasing the detectability of stealth targets [32].

The impact the RCS has on a radar measurement can be seen in the bistatic radar equation, of which a simplified version is given in (2.6), assuming no loss factors [13].

$$P_{\mathrm{r}} = \frac{P_{\mathrm{t}} G_{\mathrm{t}} G_{\mathrm{r}} \lambda^2 \sigma}{(4\pi)^3 R_{\mathrm{tx}}^2 R_{\mathrm{rx}}^2} \tag{2.6}$$

In (2.6) P_{r} is the power received at the receiving antenna, P_{t} the transmitted power, G_{t} the transmitter gain, G_{r} the receiver gain, λ the signal wavelength and σ the RCS.

2.2 Line of sight

In order to detect high altitude targets it is required that they are within the antennas vertical beam width as well as not obscured by the horizon, everything beyond the horizon will be in radar shadow. The refractive index of the atmosphere decreases as a function of altitude due to its dependence on density and temperature. As a result, the atmosphere functions as a graded index and bends the radio waves allowing them, to some degree, to follow the curvature of the earth. In radar context this means that the visible horizon is extended. It is common practice to assume an extended earth radius of a factor 4/3 to account for the atmospheric refraction [5]. However, this factor was derived mainly for ground-to-ground transmission and is less accurate when scanning for high altitude targets where more complex methods has to be utilized to determine the radar horizon [5]. Due to the bistatic geometry, a PBR system can be utilized to aid in the detection of low flying targets beyond the horizon of the transmitter [7].

A limiting factor when using commercial transmitters of opportunity is the directivity of the transmitting antenna. Usually the transmitters are directed towards the earth to illuminate urban areas, which is the case *e.g.* when using DVB-T signals. This is to avoid that too much power is wasted above the horizontal plane [8]. As a consequence, sufficiently close high altitude targets will not be illuminated and hence not be able to be detected by the radar. As well as being directed towards the earth, transmitting antennas are approximately isotropic with very low gain which further limits the effective range of the system [7]. Nevertheless, DVB-T based PBR systems have been shown to have the capability to detect targets at low altitudes up to distances of tens of kilometers [8].

2.2.1 Time of transverse across beam

The shortest time a target is located inside the antenna lobe is when it travels orthogonally to the direction of the antenna. For simplicity, the lobe is considered to be shaped as an isosceles triangle in which the base is made up of the target path. By dividing the isosceles

triangle into two right triangles and using (2.7), derived from the Pythagorean theorem, the shortest target path can be calculated.

$$x = h \cdot \tan \frac{\theta}{2} \cdot 2 \tag{2.7}$$

Here h is the distance between the receiving antenna and the target and θ is the angle for the antenna beam width. Making assumptions about plausible target distance and speed, (2.7) can be used to estimate the shortest time a target remains inside the beam. The shortest time in which a target is inside the lobe sets the limit of how long a measurement can be.

2.3 DVB-T

DVB-T signals in Sweden are allocated to 470-790 MHz in the ultra high frequency (UHF) band. Using DVB-T as a transmitter of opportunity in a PBR system offers several beneficial properties. The signals are modulated with orthogonal division frequency multiplexing (OFDM) on a bandwidth that reaches up to 8 MHz which yields a fairly good range and Doppler resolution. Furthermore, the signals are highly randomized due to closely spaced subcarriers modulated with phase-shift keying (PSK) or quadrature amplitude modulation (QAM) [9]. The randomization yields attractive properties to the ambiguity function due to the independence of signal content and time invariance [8]. It is thus highly unlikely that a repetition in the signal will occur due to the content of the signal and yield a false detection of a target. On the other hand, there are ambiguities due to pilot tones and guard intervals and if no preventive action is taken these could mask returns from real targets [9]. Another positive effect of using a DVB-T signal is that they can be decoded and recreated to create an almost noise-free signal which benefits the subsequent signal processing [7].

Since DVB-T transmitters are common, it is also possible to include several transmitters in a PBR system if they are sufficiently close to each other. This gives the opportunity to operate in a single frequency network, receiving multiple reflections of a target from different angles which could aid in target localization and tracking [7].

2.4 Processing techniques

The time difference between the reflected signal and the direct path signal can be calculated by cross-correlating the signals, which in distance corresponds to the bistatic range. The reflected time-delayed signal is affected by a Doppler shift induced by a moving target which depends on the angle and velocity of the target as explained in section 2.1.1.

The cross-correlation of the two waves is defined as in (2.8) for continuous time. For discrete time, the definition of (2.8) can be expressed as in (2.9).

$$C_{\mathrm{dr}}(t) = \int_{-\infty}^{\infty} s_{\mathrm{d}}(\tau) s_{\mathrm{r}}^*(\tau - t) \, \mathrm{d}\tau \tag{2.8}$$

$$C_{\mathrm{dr}}[n] = \sum_{m=-\infty}^{\infty} s_{\mathrm{d}}[m] s_{\mathrm{r}}^*[m - n] \tag{2.9}$$

Here $s*$ denotes the complex conjugate. s_d is the direct path signal, s_r the reflected time-delayed signal, and t the bistatic time delay. A resulting peak after the cross-correlation corresponds to the bistatic time delay.

Since the signal processing concerning radar is a known subject, several methods have been developed. A well-known and frequently used tool is the ambiguity function, defined in (2.10). By using this method both range and Doppler processing may be achieved [3].

$$\chi(t, f_d) = \int_{-\infty}^{\infty} s_d(\tau)s_r^*(\tau - t)e^{j2\pi f_d\tau} \, d\tau \tag{2.10}$$

The ambiguity function corresponds to the implementation of a matched filter. The function detect targets by estimating the bistatic Doppler shift along with the estimate of the bistatic range. Mathematically, the bistatic range-doppler function for a PBR system is evaluated as in (2.10) for continuous time. This is under the assumption that the reflected signal is a good enough copy of the direct path signal [20].

In a measurement system, the receiving devices sample the incoming signals with a sampling frequency rate, f_s. This changes the mathematical expression in (2.10) into an expression in discrete time notation as in (2.11).

$$\chi[l, m] = \sum_{n=0}^{N-1} s_d[n]s_r^*[n - l]e^{j2\pi \frac{m \cdot n}{N}} \tag{2.11}$$

Here N is the number of integrated samples, l the time bin corresponding to the delay and m the Doppler bin corresponding to the Doppler shift f_d.

An efficient implementation of the ambiguity function is the Direct Fast Fourier Transform (FFT) . This implementation has a lower computational cost and is thus faster than (2.11). Other possible implementations exist and are compared along with the Direct FFT in [20]. The algorithm is based on the observation that the Doppler frequency can be found along the samples at the l-th time bin as expressed in (2.12).

$$\chi[l, m] = X_l[m] = \text{DFT}\{x_l[n]\} \tag{2.12}$$

The resulting algorithm of Direct FFT implementation is sketched in figure 2.2. The first block indicates the bistatic delays. The second block with $x_l[n]$ is the cross-correlation in one time bin and the third is the DFFT evaluation. That is, for each one of the bistatic delays, a DFT is evaluated.
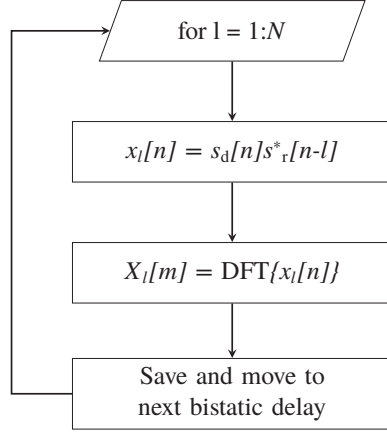
Figure 2.2: *Flowchart of Direct FFT.*

In this project the Direct FFT will be used to processes the measured signals. The PBR-system will present the estimates of the bistatic range-Doppler in a 2-dimensional color plot. With this processing technique, a moving target can be visualized by its bistatic range and Doppler frequency.

2.4.1   Range and Doppler walk

Range and Doppler walk, or migration, occurs when a target moves through multiple range or Doppler cells during the integration time. The integration time corresponds to the total number of samples that are processed for a single range-Doppler matrix. Ideally, the integration time should be adjusted depending on the target under measurement. *E.g.* slow moving targets such as maritime traffic can tolerate a long integration time without any range or Doppler walk. A long integration time also increases the signal-to-noise ratio (SNR) gain which aids in detecting low radar cross section targets. Consequently, high velocity targets require a short integration time on the order of fractions of a second to avoid these effects [8]. When determining the integration time it is thus necessary to take into account the possible velocities a target can maintain. Ideally, it should be chosen so that the target remains in the same range bin during the duration of the integration time. *E.g.*, according to (2.13), a commercial aircraft traveling with a bistatic velocity of 250 m/s, measured by a system with a bandwidth of 12.5 MHz should have an integration time less than 0.096 seconds to avoid range walk.

The increase in SNR is only valid to a certain extent, if range or Doppler migration occurs it leads to energy dispersal in the correlation, taking the total amount of energy and spreads it to multiple range and Doppler cells. These effects lowers the SNR of the measurement and also affects the resolution [3]. Whether a measurement will suffer from range walk can be estimated with (2.13), where T_I is the integration time and B is the bandwidth of the signal.

$$v_B T_I \ll \frac{c}{B} \tag{2.13}$$

If the inequality holds, the probability for range walk will be low. Similarly, if the inequality in (2.14) is satisfied, there will be a low probability of Doppler walk.

$$T_I a_B \ll \frac{c}{2f_c} \tag{2.14}$$

Here a_B is the bistatic acceleration. A longer integration time increases the Doppler resolution of the measurement, but it also increases the sensitivity to the bistatic acceleration, thus increasing the probability of Doppler walk [19], similarly as a target with a high bistatic velocity increases the risk of range walk.

Since the bistatic velocity as well as the bistatic acceleration depends on the direction of the target in the bistatic geometry, range and Doppler walk are highly dependent on the aspect angle on the target.

Chapter 3
System architecture

This chapter begins by highlighting some of the requirements that need to be fulfilled in order to conduct successful measurements of a target's Doppler shift and range. What follows is a description of each individual component in the PBR system and ends with a section describing the complete system and experimental setup.

3.1 Requirements on the system

The transmitting antenna used in this PBR system is broadcasting channels with a carrier frequency between 470 MHz and 790 MHz in the UHF band. These transmitted radio waves need to be converted into electric power by an antenna that can receive signals in this range. This makes the system customizable as it can receive signals from channels on different frequencies. Another requirement is the beam width of the antenna. The antenna directed towards the reference antenna should have a narrow beam width for a stronger reference signal, whereas the surveillance antenna should have a wider beam width in order to cover a larger potential target area. Finally, assuming that the transmitting antenna is broadcasting at a strong enough signal, losses in the receiving end should be small in order to have a good range. This includes low cable attenuation and good antenna characteristics.

The signals from both antennas are expected to go through a process where they are amplified, down-converted and filtered before they pass the analog-to-digital converter (ADC). This process should be done in a suitable receiving device. The bandwidth of the transmitted channels are 8 MHz which sets the lower sampling frequency limit for the ADC. As well as being able to achieve the necessary sampling frequency the ADC should have a high enough resolution to have a good accuracy. In order to be able to process the collected data, it is also necessary that the bandwidth between the receivers and processing computer is high enough so that the transfer can occur without errors.

It is important for the signal processing, which is explained in Chapter 2, that the two channels are recorded simultaneously. This can be achieved by using the same clock

for both channels as a reference when the signals are going through the process of down mixing and analog to digital conversions. Even if both channels use a reference clock, there will still be a phase offset in the down conversion stage. This can be remedied by measuring a known signal and compensating for the phase offset in the signal processing.

3.2 Hardware

This section describes each component, and their uses, in the PBR system.

3.2.1 USRP N200

The USRP N200 is a software-defined radio device, SDR, from Ettus Research^{TM}, a National Instruments company.

The device was chosen because of its high ADC processing bandwidth, *i.e.* sampling frequency, and the use of Ethernet interface. To achieve a broad frequency range SBX was chosen as daughterboard, which gives the possibility to set the center frequency between 400 MHz and 4.4 GHz. The device also has a tunable gain range between 0 and 38 dB.

An inherent effect of using Transmission Control Protocol/Internet Protocol-based (TCP/IP) data transfer to the host processor (due to the GigE interface) is that the SDRs basically can be located at the antennas while the host processor can be a large distance away from the actual receiving site. This because the signal is digital after the ADC, and is not as sensitive to attenuation or disturbances as an analog signal.

Another reason for the choice of USRP N200 was the possibility to add an external reference clock and a pulse per second signal (1 PPS). The PPS tells the devices the start of every second, which allows the devices to start their sampling at the same time. This was desired in order to make the post signal processing as efficient as possible. Although, the local oscillators (LOs) in the SDRs would still have a phase shift with respect to each other due to the dividers in the phase-locked loop chains (PLL). How this issue could be addressed is explained in section 3.2.4.

A simplified system diagram is shown in figure 3.1, depicting the principal functionality of the SDRs. The RF-frontend, or the SBX daughterboard, allows for both receiving and transmitting operation due to that the LOs in both chains operate independently [24]. The RF switches in the front-end also permit half-duplex operation on the transmitter port. This allows for a number of different possible antenna configurations. For this thesis only the receiving operation at port RX2 is used.
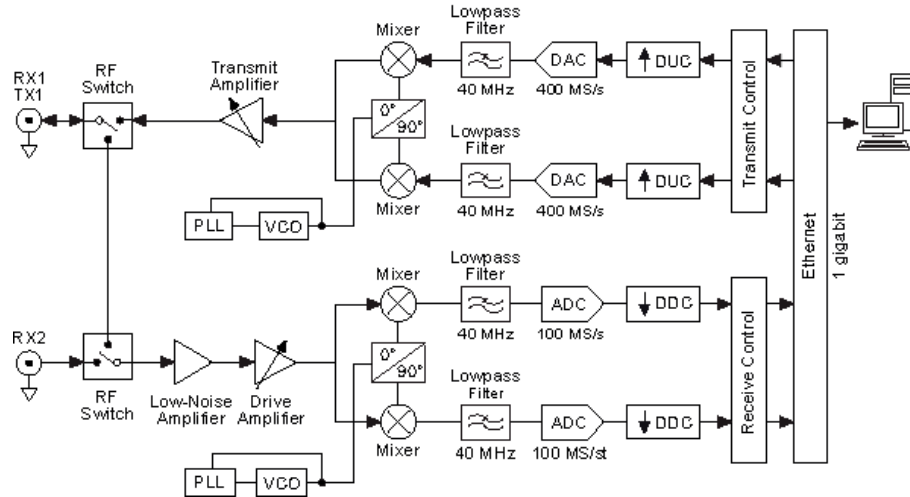
Figure 3.1: *Architecture of USRP N200 with SBX daughterboard [23].*

After the amplifying stage, the RF signal is separated and phase-shifted by 90° in the mixer into an I and a Q part. Followed by low-pass filtering the two signals are sampled at 100 MS/s in the ADC process and then down-converted at the digital down-converter (DDC) to a complex baseband signal. Usually there exist an IQ-imbalance, *i.e.* the phase shift is not precisely 90°. This imbalance is a result of the analog quadrature down-mixing and arise due to different channel environments and component properties [16].

The DDC is provided by the Field-Programmable Gate Array (FPGA) image which also includes fine-frequency tuning and filters for decimation [23]. Eventually, after some further processing, the samples are sent to the host computer.

Characterization

In order to have an estimate of the performance of the USRP N200 a SNR measurement was made using the full scale of the resolution. During this measurement a sine wave from a state of the art signal generator with very low spectral sidebands were used to minimize the noise contribution from the signal generator. For this purpose a large number of FFT-points were also used, one million points for a signal length of one million samples, collected with a sample frequency of 12.5 MHz.

The ADC in the USRP has a resolution of 14 bits. It is however after the internal processing represented as 16 bits due to conversions and scaling factors [31]. Most likely in order to facilitate the data transfer as two full bytes. This is confirmed in figure 3.2 showing the total number of excited bits at around $\pm 2^{15} = \pm 32768$, indicating full scale.

During the measurement the signal generator generated a signal at 475 MHz and the center frequency of the receiver was set to 474 MHz. Normally the shape of the his-

togram for a sine wave should be U-shaped, but since the baseband signal has a rather high frequency of 1 MHz, compared to the sampling frequency of 12.5 MHz, there are not sufficiently many samples per period to properly recreate the signal for these purposes. Instead the samples recur somewhat periodically at the same location during each signal period as shown in the histogram.
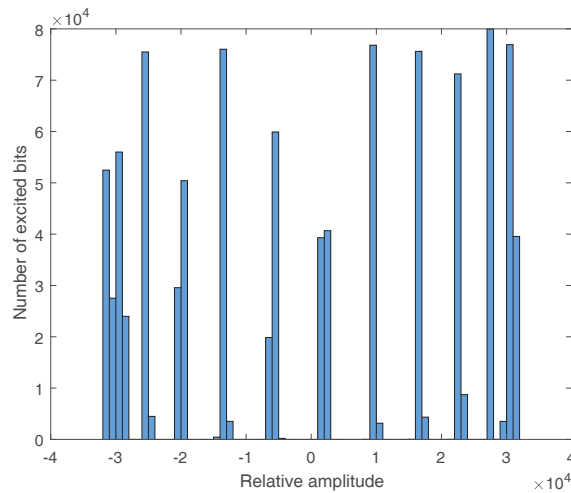

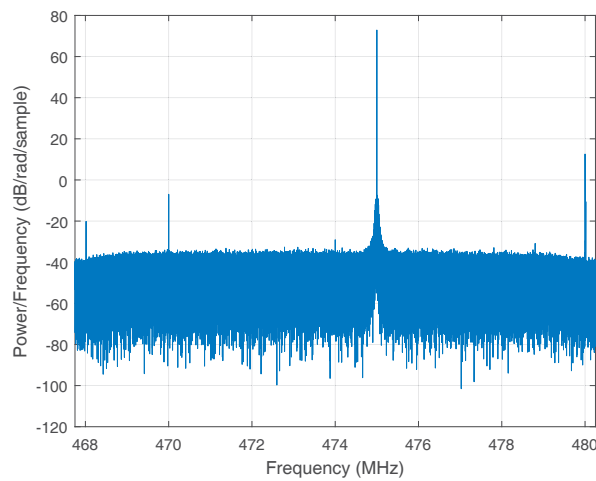**Figure 3.2:** *A histogram of the SNR measurement indicating full scale.*

Figure 3.3: *Power spectral density estimate at the center frequency 474 MHz with a signal at 475 MHz.*

Figure 3.3 displays the power spectral density estimate of the generated signal. Excluding the signal there are also spurs at 468, 470 and 480 MHz, which are always present at the 474 MHz center frequency and hence not signal dependent. These could presumably originate as a result from the mixing process or from multiples of the LO frequency. Since these spurs are located outside the signal bandwidth of 8 MHz they can be safely removed without affecting the results from subsequent live measurements, including the spur close to 470 MHz. Also visible is the direct current-component (DC) at the center frequency due to leakages in either the LO or the low-noise amplifier [22].

The SNR was obtained by using the amplitude spectrum and dividing the signal root mean square-value (RMS) with the noise RMS-value, yielding a SNR of 53 dB. This was accomplished after removing the spurs and DC-component.

Since the full scale of the receiver was used the spurious-free dynamic range (SFDR) could be measured directly from the amplitude spectrum to be 41 dB when comparing with the sidebands next to the signal. Since the measurement was performed with a clean spectral signal the sidebands close to 475 MHz in figure 3.3 is most likely a result of imperfections in the ADC. Figure 3.3 shows the power spectral density estimate and thus gives the SFDR increased by a factor two at approximately 82 dB. Due to the clean signal from the signal generator these sidebands are a result from imperfections in the AD converter.

Figure 3.4 depicts two measurements without any signal used at two different center frequencies. As with the 474 MHz center frequency, the resulting spurs are always present at their respective frequencies, even though the RF-ports are terminated with appropriate impedances. Consequently, each center frequency has their own set of spurs, at frequencies depending on the center frequency. This shows that the potential to use certain center frequencies with the required 8 MHz bandwidth without any imperfections is limited.
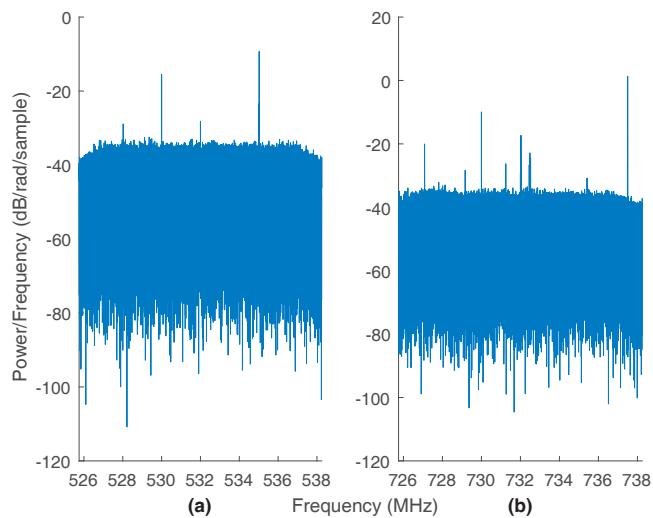

Figure 3.4: *Power spectral density estimate without any signal at two different center frequencies measured by an USRP N200. In (a) it is 532 MHz and in (b) it is 732 MHz.*

3.2.2 Octoclock CDA-2990

The octoclock CDA-2990 is a complementary device, also from Ettus Research^{TM}, that aligns the SDRs with a common reference clock. Up to eight devices can be connected and aligned which allows for coherent operation. This is accomplished by distributing a 10 MHz clock reference and a PPS signal. The octoclock used in this project could either use internally created signals or an external input, whereas the former was used for the reference clock. For higher accuracy, a Global Positioning System (GPS) antenna was used to provide for an external PPS signal.

3.2.3 Radarcape, ADS-B receiver

The ADS-B uses Global Navigation Satellite System (GNSS) to determine the host air-craft's position. The ADS-B transceiver then sends this information along with, *e.g.* the aircraft's speed, heading, altitude and flight number to both eligible ground based or air-borne receivers and to satellite communication transceivers which relays the information to traffic control centers [29].

The device used for the purposes of this thesis was the Radarcape, a passive ADS-B receiver, developed by Günter Köllner Embedded Development GmbH [17].

In addition to its own antenna, the device also uses a GPS-antenna to be able to syn-chronize the received information. Each position is thus bound to a specific time stamp and could be compared to the data collected through the PBR system in order to verify that the system was functioning correctly.

3.2.4 Switch

In order to make certain that the received signals would be synchronized, the offset was determined with the use of a number of calibration measurements made with a signal generator. This had to be done in conjunction with each measurement session and to avoid to physically change the cables a switch were used. The switch was manually controlled by the user via a USB-connection to the computer.

3.2.5 Antennas

For simplicity, the same type of antenna was used for both the reference and surveillance antenna. They had a gain of 19 dBi and a beam width of 27° [30]. These are regular TV-antennas that have a frequency range between 470-790 MHZ and can be bought in a local electronics store. The specific model used during this thesis was the DAT-HD 75 BOSS 790 from Televés.

The frequency range could be verified by connecting the antennas to a spectrum an-alyzer, viewing the full spectrum as in figure 3.5. The frequencies marked on the x-axis corresponds to the carrier frequencies for potential channels that can be used for radar measurements, each with a bandwidth of approximately 8 MHz. For this thesis the carrier frequency at 474 MHz was used for measurements, for which the bandwidth is shown in figure 3.6.
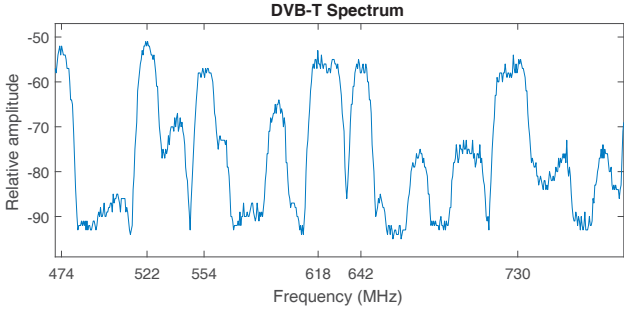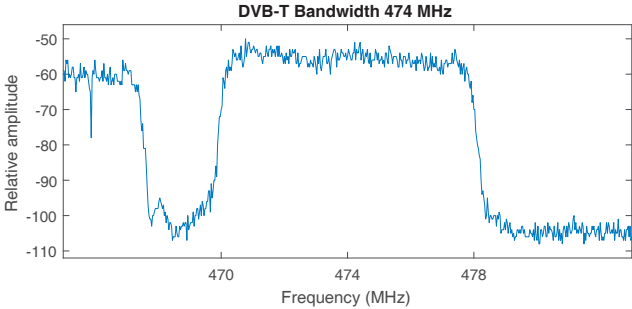
Figure 3.5: *Full span of the DVB-T spectrum.*

Figure 3.6: *Bandwidth of the channel used.*

3.2.6 Cables

The received signals were led from the antennas to the two receiving devices via two low-attenuating cables of the type RG-214. Figure 3.7 shows the characteristics of an eight meter long cable, illustrating the attenuation for the antennas whole frequency range. This diagram shows that the attenuation is less than 1 dB at the center frequency used for this thesis with an eight meter long cable.
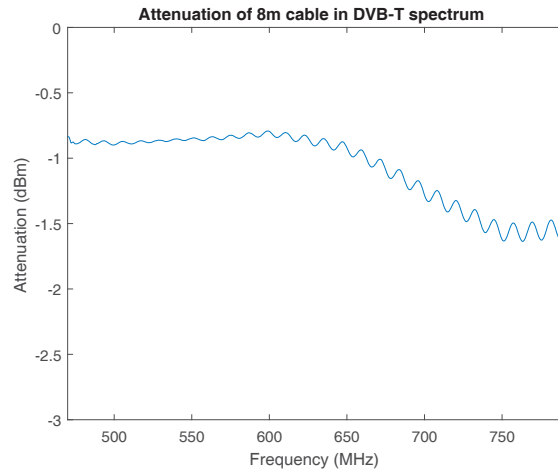
Figure 3.7: *Cable attenuation.*

3.3 Experimental setup

In this PBR system, two collocated receiving antennas were used, one that was directed towards the transmitting antenna and the other towards a potential target path. These antennas were mounted on an iron mast as seen in figure 3.8 on the roof of a van provided by FOI, and connected to the USRP devices with cables via a switch.

Figure 3.8: *Mounted antennas during a live measurement.*

The switch was also connected to a signal generator for calibration purposes as mentioned in section 3.2.4. A Windows computer was controlling the switch with a USB-connection by shifting the position of the switch between the calibration signals and the signals from the actual measurements.

The USRPs were connected to a Linux computer via an Ethernet interface, with each device on a separate network. With a total of four NICs, two of these were thus occupied by the USRPs, one by the Radarcape and the fourth by the router connecting the computer to the LAN.

The LAN consisted of the Linux and Windows computers, the octoclock and the router, which also had Internet accessibility from a wireless modem. Internet access was a necessity in order to have a functioning interface when viewing the flightpaths provided by the Radarcape. The Radarcape also had a receiving antenna for the ADS-B signal.

Two GPS antennas provided accurate timestamps to the octoclock and Radarcape separately and in turn the octoclock provided the USRPs with a 10 MHz reference and PPS signal. As well as a 10 MHz reference to the signal generator. The block diagram of the complete setup is shown in figure 3.9 and the assembled system at a measurement is shown in figure 3.10 where it is mounted in the back of the used van.
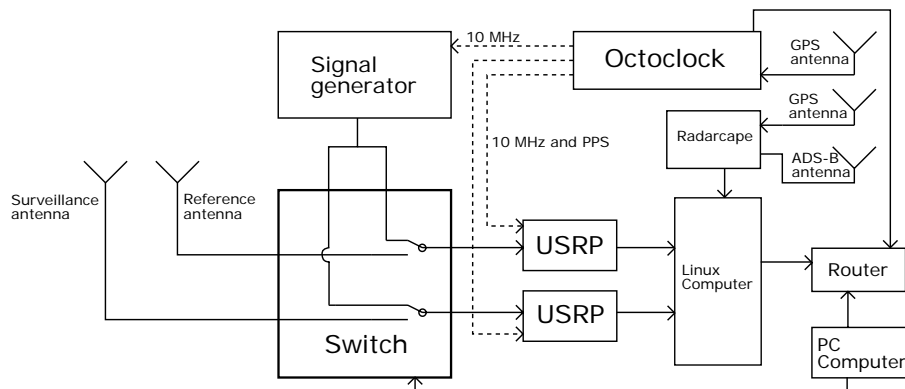
Figure 3.9: *Block diagram of the PBR system.*

Figure 3.10: *The assembled PBR system during a live measurement.*

According to the Nyquist-Shannon criteria the signal should be sampled at a rate higher than 16 MHz to achieve a reasonable reconstruction of the signal. It was decided that the sampling frequency would be 25 MHz, and since this PBR system utilizes both the I and Q part of the signal an efficient sampling rate of 12.5 MHz could be set during live measurements. Each sample corresponds to an effective size of 20 bits with 8 bits for the I and Q part respectively, where each part also has 2 control bits. By using 12.5 MHz as sampling frequency the transferred data then amounts to 250 MB/s, and 500 MB/s when using 25 MHz. Thus, considering the sampling rate of 100 MS/s in the ADC process the decimation factor was 8 and 4, respectively.

For comparison with the spectrum obtained by the spectrum analyzer in figure 3.6, figure 3.11 shows the DVB-T spectrum at 474 MHz sampled by one of the USRP's. The spectrum is within the bandwidth used during this project of 12.5 MHz. As an artifact from the processing in the USRP, two very high-level spurs are visible, which are always present when the center frequency is 474 MHz. Fortunately, these frequencies are outside the signal of interest and can be safely removed without altering anything within the desired 470-478 MHz interval.
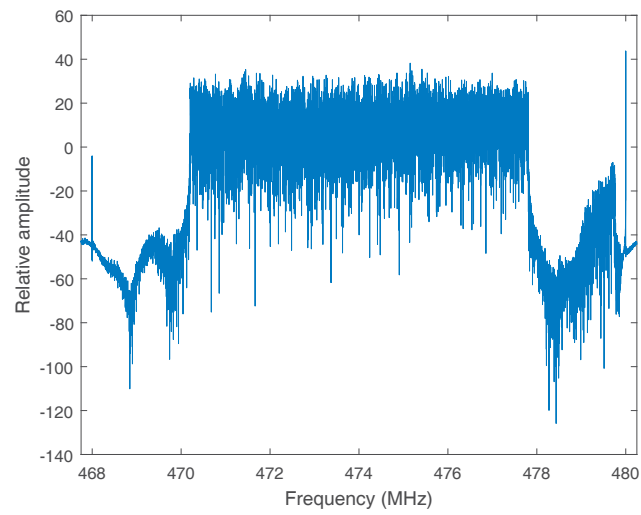
Figure 3.11: *Spectrum at center frequency 474 MHz measured by an USRP.*

Chapter 4
Software implementation

The following chapter describes the implementation of the software. It is divided into three sections where the first section describes an initial attempt to operate the system with MATLAB. This method turned out to be ineffective for the purposes of this thesis, instead this was done with C++ on a Linux computer and is explained in the second section. The third and last section describes the implementation of the code used for the signal processing which was done in MATLAB on a Windows computer.

4.1   Initial MATLAB attempt

Initially the system was supposed to be configured and operated with MATLAB on a Windows operating system. Alas, during the configuration and testing process it was realized that the available functions that could be used in MATLAB were insufficient for the purposes of this thesis. The level of accuracy needed for the system regarding the synchronization of the devices, was to the knowledge of the authors of this thesis, not obtainable with MATLAB. Mainly because of arising difficulties when trying to start the streaming process to collect data in multiple USRP's at the same time. Additionally, the USRP N200 was initially developed to be used by Linux based systems whereas Windows was, during the time of this thesis, not fully supported. Unfortunately, the difficulties of using MATLAB on Windows was not realized until after a fully operational program was developed for the basic functions of the USRPs. A figure showing the graphical user interface of the program is shown in figure 4.1. All relevant parameters could be entered in the GUI and it also had the possibility to synchronize the devices and to start the streaming process. It thus had all the necessary functions needed to collect data.
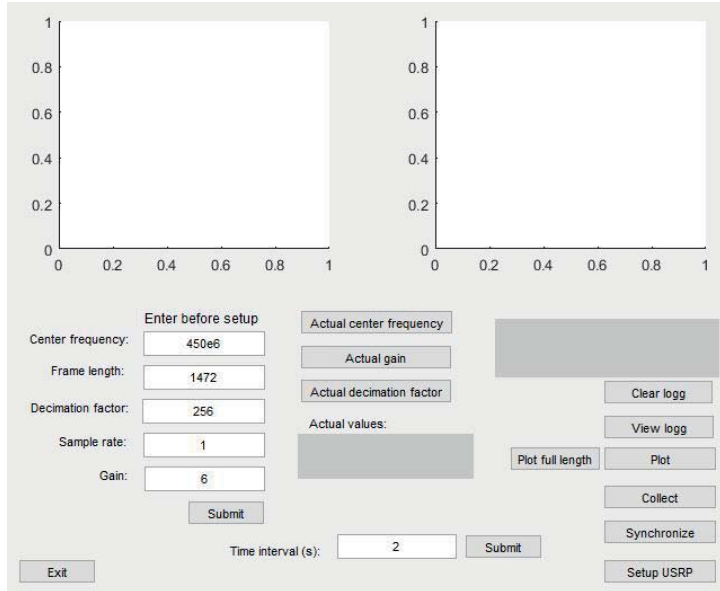
Figure 4.1: *GUI of initial* MATLAB *program.*

4.2   C++

The Linux computer used the USRP Hardware Driver (UHD) software utilities and modified C++ example code from the UHD software. This enabled configuration and start-up of the USRPs, including setup and synchronization using CDA-2990 of the devices, transfer of input parameters such as center frequency, gain, buffer size, duration of streaming and to start the actual streaming process.

The data was sent from the USRPs in a *short* format which means that each sample had a size of 4 bytes, where both the I and Q part is depicted with 2 bytes each, excluding the four control bits.

The receiving process in the program is contained in a while-loop that is running until the desired duration has been satisfied. Each receive command then collects an amount of samples corresponding to the allocated buffer size set in the configuration process and saves the data to a file. Thus, the data are collected and saved in segments corresponding to a predetermined value.

To maximize the efficiency a solid state disk (SSD) was used with a high write-to-disc speed and the maximum buffer size was used.

The subsequent subsections describe what the program does when executed according to the flowchart in figure 4.2. A user manual of how to run the program is included in appendix A. In addition to the program options presented below there also are minor options not presented here. Among these are the ability to test if the devices are synchronized and the option to enter flight names observed in the Radarcape interface to collect information about the flight paths.
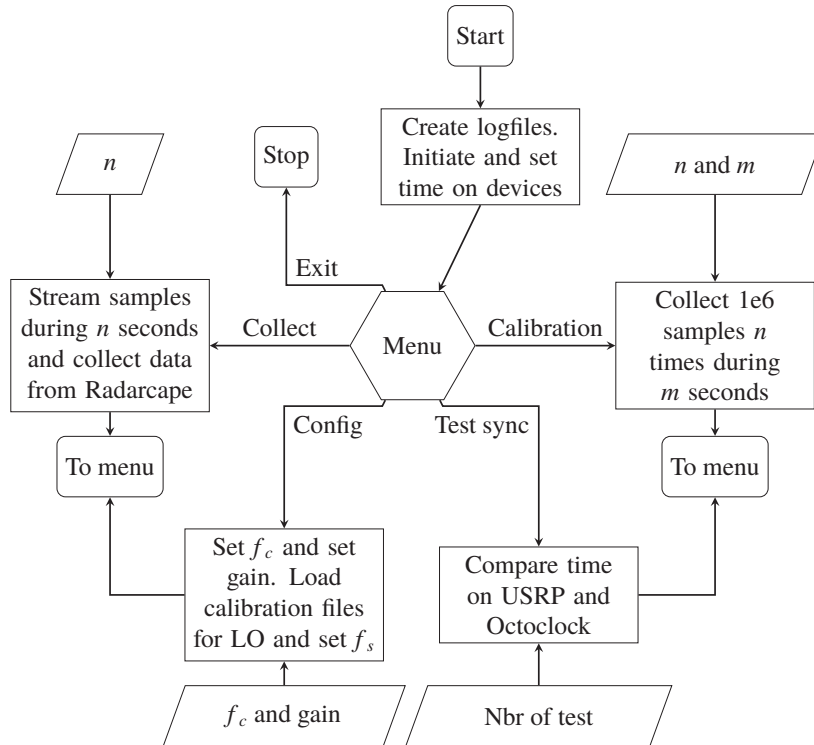
Figure 4.2: *Flowchart of the C++ code.*

4.2.1 Start up

At start up, the log files are created and the devices are initiated. The current time is retrieved from the octoclock and sent to each USRP to align the devices. In addition, both USRP devices are set to use the external 10 MHz reference clock and the PPS-signal provided by the CDA-2990. After these initial steps, the next option may be selected in a menu.

4.2.2 Configuration

In the configuration process the user sets the gain and center frequency. The frequency is set by using timed commands to ensure that both the USRPs receives the command at the same time. This aligns the LOs in each front-end, ensuring that the phase offset remains constant [25]. This offset is entirely random, and aligning the USRPs are crucial in order to allow for successful measurements with a level of accuracy that this thesis requires.

During the frequency configuration process, calibration files are loaded into the US-RPs. These files were made during the initial pre-measurement configuration of the USRPs and contains results from a self-calibration. By using the calibration files the IQ imbalance and DC offset are minimized.

4.2.3   Calibration

Even after taking the afore-mentioned steps in section 4.2.2 to ensure that the USRPs are aligned, there still exists a phase difference between the LOs in each front-end. To compensate for this, calibration measurements are necessary, assuming that the offset remains constant for a sufficient duration of time. These measurements are made in conjunction with target measurements with the use of a signal generator transmitting a sine wave with a known frequency. The results from these measurements are used during the signal processing to shift one of the signals in order to align them.

   The user specifies how many calibration files should be taken and the time interval between each measurement. Each calibration measurement is hard-coded to collect one million samples. The sample frequency is also hard-coded to be 25 MHz.

4.2.4   Collecting data

One of the main benefits of using C++ instead of MATLAB was the ease of issuing the stream command to both the USRPs simultaneously. This should ensure that the measured bistatic delay is not erroneous due to a time difference in the streaming process. The preceding steps along with simultaneous streaming should allow for a reasonably accurate measurement.

   The user specifies how long a measurement should be, but due to the large amount of data that needs to be processed, a measurement has not been longer than a couple of seconds during this thesis. The sampling frequency can also be specified by the user, but has been chosen to be half that of the valued used during calibration measurements, 12.5 MHz. This is because it is possible to use the whole IQ pair instead of just the I or Q part, which is not possible for a sine wave.

4.3   MATLAB

After a measurement is completed, all calibration and measurement files are transferred to the Windows computer and processed with MATLAB. This is done by a script using Putty.exe and Secure copy. The copied files are paired in such a way that the first index of the measurement name represents the order of measurements and the second indicates if it is from the reference or surveillance antenna. The MATLAB program is divided into three scripts for processing the signals. Figure 4.3 shows the flowchart of the MATLAB scripts and the coordination of the program.

4.3.1   Calibration

The calibration script reads the values from binary files and sorts the complex signals. The complex signals are then evaluated in the cross-correlation function from the signal processing toolbox. By measuring signals generated by a signal generator, the real and imaginary parts are evaluated separately. The cross correlation function estimates the phase-lag between the LOs in the USRPs in each calibration file and saves the mean-value

of all calibrations. This value is then used to adjust the LOs offset for one device relative to the other.

Spurs in the calibration signals were removed by transforming the signals into the frequency domain and damping the frequency bins corresponding to the spurs.

4.3.2 Sorting

Similarly to the calibration script, the sorting script also reads the values from the binary signal files and sorts the complex signals. The number of samples is not a fixed number as in the calibration script and therefore sorted differently. Each measurement consists of two complex signals, one from each antenna. The signals are sorted as matrices where each column represents a time interval. Due to the importance of symmetry in the matrix and the irregularity in the number of samples, redundant samples in the end of each sample vector are discarded. The size of the matrix depends on the bistatic range of interest.

4.3.3 Range-Doppler

The range-Doppler script is implemented as described in Chapter 2.4. It starts by compensating for the LO offset with the value from the calibration script. This is done by multiplying one of the complex signals with a complex number corresponding to the value for the phase difference. It is important that the absolute value of the complex number is equal to one since the amplitude of the complex signal should remain the same. Each column in the signals is then multiplied with a Blackman-Harris window to reduce spectral leakage and then the two signals are cross-correlated column wise. The positive half of the correlation between each column in the signal matrices is stored as a row vector in another matrix. The duration of one row is interpreted as a slow-time, the inverse of which is the sample frequency after the correlation. Each column in the resulting matrix is again multiplied with a Blackman-Harris window, this mitigates the effect of range walk due to long integration times.

The n-point DFT is then computed with the FFT function from the MATLAB processing toolbox, where n was chosen to be 256. Each column is thus evaluated column wise with 256 rows for each FFT. The value of n determines the Doppler resolution in the range-Doppler matrix and n times the slow-time is the total integration time of the process. The resulting matrix is a range-Doppler matrix where each element represents a pixel value. This matrix is plotted in a colormap that uses the full range of colors. A pixel with a high value indicates an echo received by the surveillance antenna corresponding to the range and Doppler values of that pixel. Stationary targets will thus be located at zero Doppler shift and moving targets will either have a negative or positive value at a corresponding distance.

The bandwidth of the DVB-T channel used for processing the signal was 8 MHz. The receiving devices have a bandwidth of 12.5 MHz which yields 4.5 MHz of unnecessary frequencies. Similarly to the spurs in the calibration files, the unnecessary frequencies were removed from the signal.
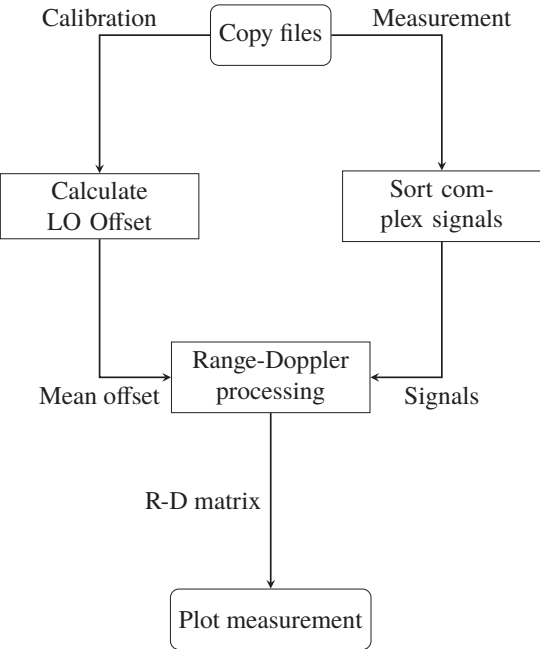
Figure 4.3: *Flowchart of the* MATLAB *code.*

Chapter 5
System verification

The timing is a crucial part in a PBR system. The efficiency of the processing algorithms depends on that the two devices are synchronized and collect the samples simultaneously. To achieve this each USRP had to be internally synchronized and aligned to each other. An estimate of the stability of the synchronization should also be known, to give an indication for how long these properties hold with respect to drifting. This chapter describes the synchronized sampling, the internal synchronization, the calibration process and the stability of the LOs. It also includes results from testing these properties. These tests were done on the final measurement system to know if the system meets the requirements set out in this thesis.

5.1   Synchronized sampling

In order to start measuring the direct and the reflected signal simultaneously, the PPS pulse from the GPS-signal along with the 10 MHz reference signal generated from the Octoclock where used. The start up sequence in the C++ program tells the receiving devices to use an external reference clock, *i.e.* the 10 MHz signal generated from the Octoclock, as well as aligning them with the use of the PPS signal. This initiation step in the program synchronizes the two devices in time. This setup gives the possibility to add multiple devices that can be synchronized due to the total of eight outputs on the Octoclock. An alternative method for synchronization is to connect the devices through a cable and setup a Master/slave model. The cable shares the time and reference properties from one device to the other to make sure the devices are synchronized. This method was not used since only two devices could be connected this way, limiting the expandability of the system.

The synchronization were verified with a LFRX daughterboard inserted in both the USRP devices. Unlike the SBX daughterboard which were used for the final system, the LFRX daughterboard does not have a LO or down converter and can accept DC signals. Figure 5.1 shows a ramped signal generated from a signal generator which was connected

to both USRPs via a signal divider and two equally long cables. The signal had a duration of 0.2 seconds and was sampled at a rate of 10 MHz. By examining the peaks at a higher resolution it was noted that they occurred at the same time for each USRP, verifying that they have simultaneous sampling with an accuracy of 100 ns.
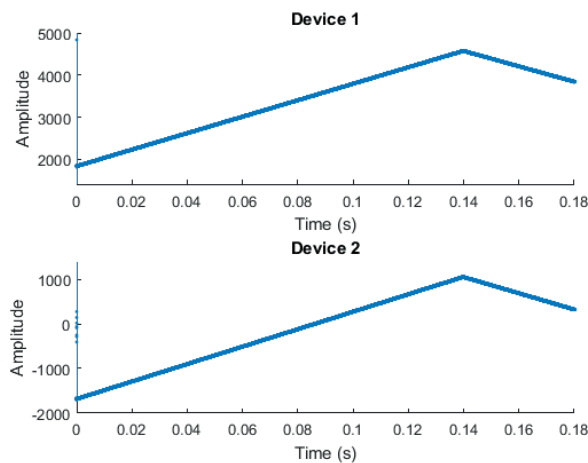

Figure 5.1: *Synchronized start of both devices.*

The difference in amplitude could be due to the signal divider, which does not necessarily distribute the power from the signal generator equally across each cable or because of differences in the characteristics of the LFRX cards. This does not affect the test of the synchronized sampling in figure 5.1 since the signal power is irrelevant in this case. Although the devices start streaming simultaneously there still exist a phase shift when using the SBX card due to the internal LOs of the daughterboard.

5.2 Internal synchronization and calibration

There are utilities in the UHD software that calibrate the devices. The difference in phase between the output from the A/D converter, I and Q, should be phase shifted by 90° for efficient processing. Initially the devices phase shift deviated from this value and reached around 87° after using the aforementioned utilities.

With the USRPs calibrated and the simultaneous sampling verified, the difference in phase between the signals from the two USRPs can be noticed in figure 5.2, showing the real and imaginary parts separately. The phase difference between the LOs of the daughterboards should remain fairly constant, at least for a certain amount of time, due to the timed commands used in the software as mentioned in section 4.2. This allows for the LOs to tune in to a frequency and become locked with a certain phase. The difference occurs because of the autonomy of the LOs. Even though they are tuned to the same

frequency they will still have a random and unique phase with respect to each other. Thus, if both the USRPs would operate with the same LO this problem should not occur.
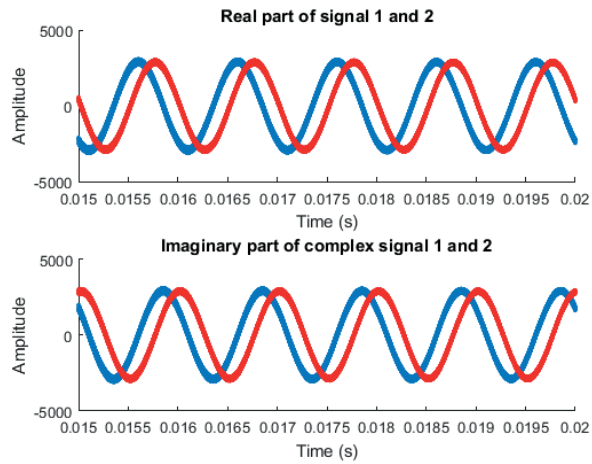

Figure 5.2: *Two complex signals with noticeable phase difference.*
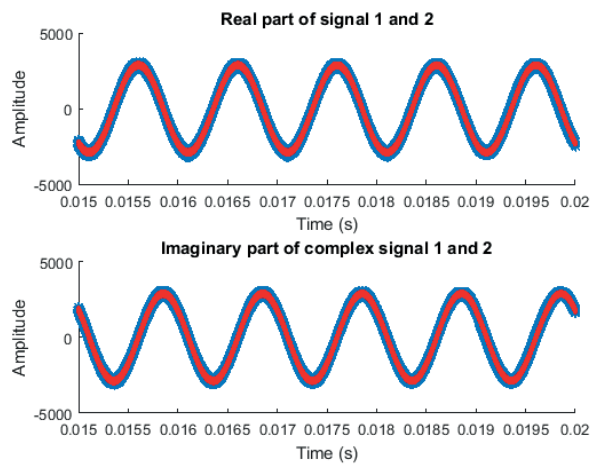

Figure 5.3: *Two complex signals where one has been phase shifted.*

Similar to when analyzing the synchronized sampling, the LO offset was measured by splitting a sine-signal generated from a signal generator and sampling them at a frequency

of 25 MHz using equally long cables. As this calibration is part of the final system the SBX daughterboard was used. The offset in figure 5.2 was measured to be approximately 60° and by using the calibration measurements described in section 4.3 this phase difference was used to align the signals. The result of this is visible in figure 5.3.

Due to the randomness of the phase difference the calibration must be done explicitly for each measuring season.

5.2.1 Stability

As the local oscillators change their characteristics depending on the temperature and other factors, a stability test of the system had to be made. Although the receiving devices are collocated, the LO of each daughterboard change independently. The duration for the stability test was one hour. A C++ program was written to automatize the test where every twenty seconds a signal was measured for 40 ms. The LO offset was then calculated for each measurement which resulted in 181 different angles for one hour. The first six phase offsets where used to get a mean value of the offset. This mean value was then used to phase shift every signal measured during the one hour stability test. The reason to use only the first six angles for the mean value was to mimic a typical measurement as it was intended. That is, measure a known signal generated from the signal generator and calculate the phase offset between the SBX cards in the receiving devices and then manually shift one of the signals obtained from a target measurement.

In figure 5.4 and 5.5 the angle offset in mrad is shown for one hour, each from a different measurement. The measurements plotted in the figures are independent of each other and are therefore showing the typical drifting of the offset. Note that each offset has been phase shifted with the mean value of the first six angles before plotted in the figures. The average error in figure 5.4 and the standard deviation where similar to those of figure 5.5. The average error in figure 5.5 were 0.8 mrad and the standard deviation for the error were equal to 2.2 mrad.

This concludes that the system is working properly with respect to simultaneous and coherent sampling and that the phase should not drift an unreasonable amount during the time needed to conduct measurements.
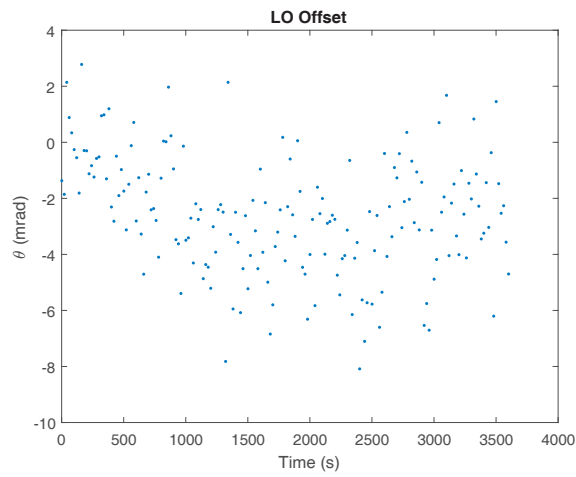
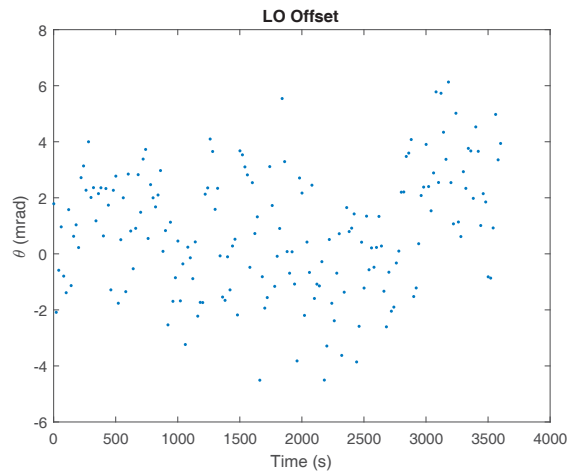**Figure 5.4:** *LO phase offset measurement 1.*

Figure 5.5: *LO phase offset measurement 2.*

Chapter 6

Simulation

This chapter describes a simulation that was carried out with a modified version of the code used for the signal processing. Since apparent targets did not seem to be easily detected by the system in early tests, the simulation was an important tool to verify that the processing code was executed properly.

6.1 Implementation

A segment of the DVB-T signal that had been collected by the reference antenna was used as a source during the simulation. The signal was copied, delayed and applied with a Doppler shift in order to mimic a reflected signal. The purpose was to simulate a moving target traveling at a constant velocity with a straight flightpath through the center of the baseline in a hypothetical bistatic geometry. This configuration was chosen because of the ease of implementation and to have an easy comparison with theoretical results. In the vicinity of the baseline the Doppler shift should be small because of the large bistatic angle. When the target is far away compared to the distance of the baseline the geometry is quasi-monostatic and the Doppler shift should represent the targets almost full velocity.

The hypothetical target had a velocity of 90 m/s. Every five seconds a measurement was taken with a duration of one second. At each new measurement the bistatic range was calculated and used to determine the delay which increases the separation of the two signals. The total traveled distance of the reflected signal, $R_{tx} + R_{rx}$, was used to determine the change in distance between each measurement and then applied in (2.5) to determine the Doppler shift. The reflected signal was then shifted according to (6.1), multiplying each element in the signal with a Doppler dependent exponential, where S is the signal and n the index of the signal.

$$S(n) = S(n) \cdot \exp\left(\frac{j\pi n f_d}{f_s}\right) \tag{6.1}$$

Furthermore, to simulate the decrease of signal power as a function of distance, the bistatic radar in (2.6) was utilized. The transmitting antenna had a signal power, corresponding to the one used during live measurements, of 2 kW and a gain of 0 dB. The receiving antenna had a gain of 19 dB and to simplify the implementation the RCS had a constant value of 100 m^2.

At each simulated measurement the proper delay and Doppler shift were applied, as well as attenuating the reflected signal with the use of a simplified version of the bistatic radar equation. However, the Doppler shift and range remained constant during the duration of a measurement which is not a realistic reflection of real targets. In order have a better representation the signal matrix was constructed in a way that gives an integration time of 0.6 seconds. Inserting this value with the inequalities in (2.13) and (2.14) shows that range and Doppler walk had a high probability of occurring if the target would have been real.

For each simulation displayed in this section, all associated simulated measurements have been added together in linear scale and inserted in the same plot where they are displayed in logarithmic scale.

6.2 Results

Figure 6.1 shows twelve consecutive measurements incorporated in a single range-Doppler plot, where the Doppler frequencies have been converted to bistatic velocity with (2.4). The baseline is 5 km of which the target starts 1350 meters below the center point, and then travels in a straight path continuing beyond the baseline. As illustrated in the figure the magnitude of the bistatic velocity varies depending on the bistatic geometry, especially in the vicinity of the baseline where it tends to zero.

As is clearly visible, there are some spreading into surrounding bins. Since the injected range and Doppler shift remain constant these are artifacts from the FFT process as a result of the long integration time and not an effect from the simulated target.

A second simulation was carried out in order to illustrate the quasi-monostatic case. Here the baseline is 1 km and the target starts 1800 meters away from the center of the baseline and then continue further away in a straight path. Figure 6.2 shows three consecutive measurements in the same range-Doppler plot, where again the Doppler frequencies have been converted to bistatic velocity. As shown, at these distances the targets velocity component approaches the targets true velocity of 90 m/s.

The results from the simulation correspond well with how a real target should be displayed according to Chapter 2 for a similar bistatic geometry. This indicates that the signal processing should be properly implemented to be able to measure bistatic range and velocity.
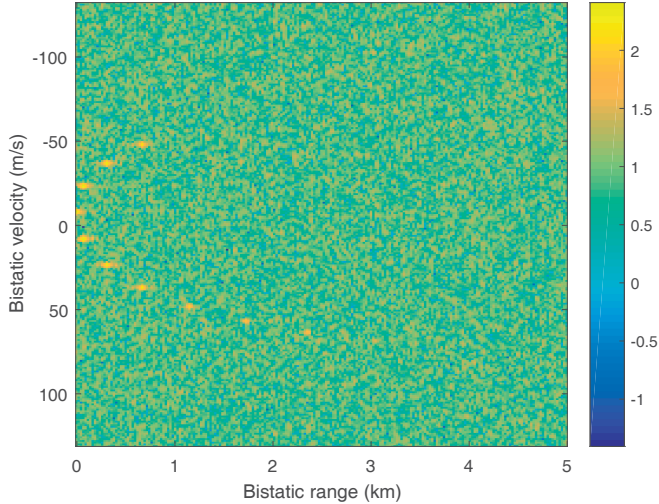
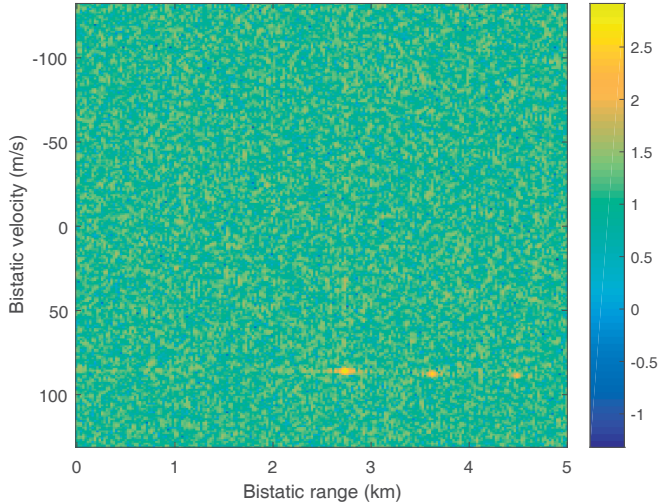**Figure 6.1:** *Range-Doppler plot of simulation. Baseline equal to 5 km.*

Figure 6.2: *Range-Doppler plot of simulation. Baseline equal to 1 km, quasi-monostatic case.*

Chapter 7
Live measurements

This chapter presents the results from successful measurements carried out on live moving targets as well as describing the bistatic geometry for each measurement. Two different sites were used for these measurements, one for a landing commercial aircraft and one for an Unmanned Aerial Vehicle (UAV) . The chapter begins with a summary concerning the range-Doppler plots and ends with a section describing a method for "ground truth" using the Radarcape. At least for the commercial aircraft this would have been used to validate the measurements, had only the target been detectable by the Radarcape.

7.1   Range-Doppler images

The result of the signal processing method presented in section 2.4 is presented as a 2-dimensional matrix where each element represents a combination of Doppler shift and the strength of the correlation, *i.e.* the bistatic range. This is visualized as a range-Doppler image where the Doppler shift has been converted to bistatic velocity with the use of (2.4), as already seen in Chapter 6. The sign of the Doppler shift depends on the moving target, which shifts the carrier frequency of the reflected signal depending on what direction the target has. If the target travels toward the center of the baseline the Doppler will be positive and negative if moving away. After transforming the Doppler shift to velocity the sign will be the opposite according to convention.

As explained in section 2.1 the bistatic range corresponds to the time difference between the signals received at the reference and surveillance antenna and does not represent the target's true distance from the measuring site. Since stationary targets do not give rise to any Doppler shifts these will be represented at the zero Doppler. These have been removed in order to avoid that they drown moving targets with low power, making them undetectable against the background noise. At a short bistatic range and low Doppler frequency there could also be contributions from the direct signal path, leaking in through the side lobes of the surveillance antenna. Hence, the first fifty meters are also removed.

In order to further increase the visibility against the background noise a minimum limit was set in the color plots, only allowing peaks above a certain threshold to be displayed.

7.2 Commercial aircraft landing at Linköping airport

This measurement was carried out at the edge of the landing strip at Linköping airport as shown in figure 7.1. The blue marker indicates the location of the measuring site, the white marker the location of the transmitter and the red line is approximately the flightpath of the landing aircraft. The surveillance antenna was directed in the opposite direction of the landing strip, almost orthogonal to the baseline which had a length of approximately 1.95 km. The reference antenna had an unobstructed view of the transmitting antenna.

The aircraft was a two-engine jet plane, Embraer ERJ-190, that has a wingspan of 28.72 meters, length of 36.24 meters and height of 10.28 meters [14]. These dimensions are larger than the system's range resolution of 24 meters, which makes range walk a high probability even for short integration times.

Figure 7.1: *Geometry during the measurement at Linköping airport. The white marker is the location of the transmitter, the blue marker is the location of the receiving antenna and the red line is the approximate flightpath of the aircraft.*

The results from the measurement are displayed in figure 7.2. Each image represents

a timespan of 0.8 seconds from a two second long measurement, *i.e.* an integration time of 0.8 seconds were used. Following the numeric ordering it shows a moving target approaching the baseline. The decrease in velocity is contributed by both the decrease of velocity of the target during descent and by the increasing bistatic angle.

In the vicinity of the surveillance antennas direction were also roads and even a highway. Therefore, it is most probable that the low velocity targets at short distances are reflections from vehicles transversing the beam. Although some may have been incurred due to ambiguities during the processing.
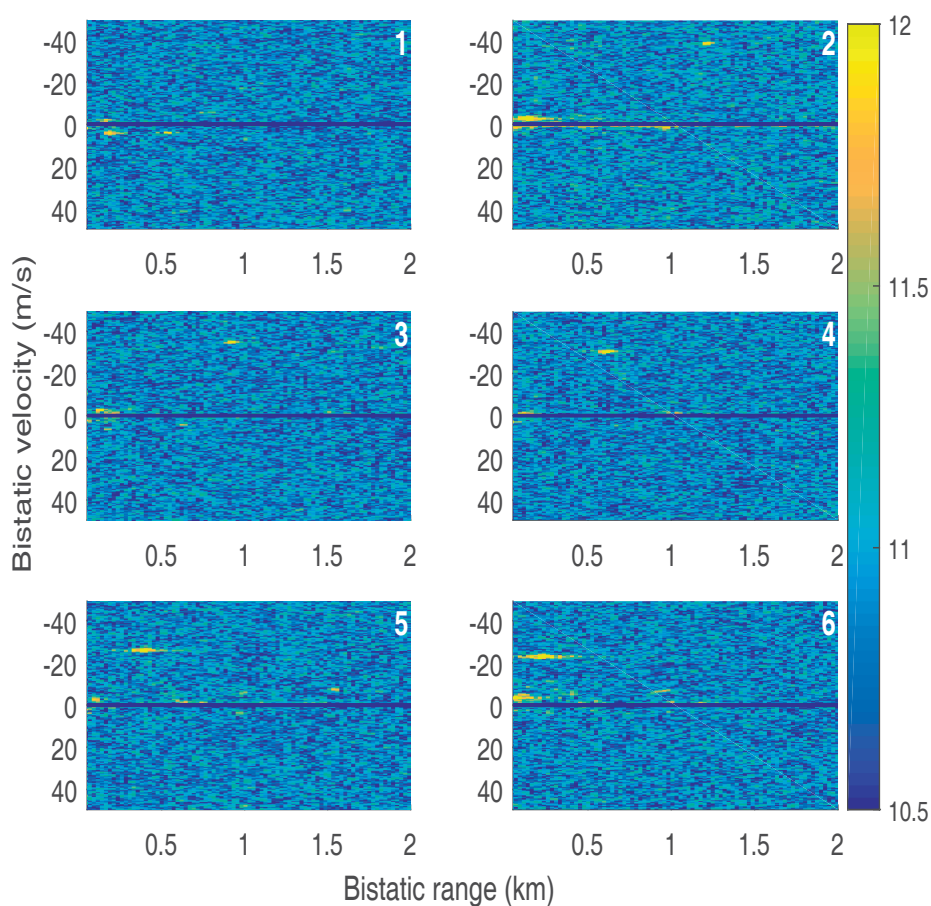

Figure 7.2: *Range-Doppler results from the measurement at Linköping airport.*

The reference USRP had been configured to have an additional signal gain of 12 dB and the surveillance USRP an almost sixteen times, in absolute values, larger gain of 24 dB.

As is clearly noted the main target is not visible in the first figure. Previous measurements on the target further away did not detect any target which indicates that the range of the system is limited.

7.3   UAV measurements

The geometry during the UAV measurement is shown in figure 7.3. Once again the blue marker indicates the measuring site, the white marker the location of the transmitter and the red lines are the approximate flight paths of the UAV where it flew back and forth. Also during this measurement the reference antenna had an unobstructed view of the transmitting antenna that were located approximately 2.95 km away from the measuring site.
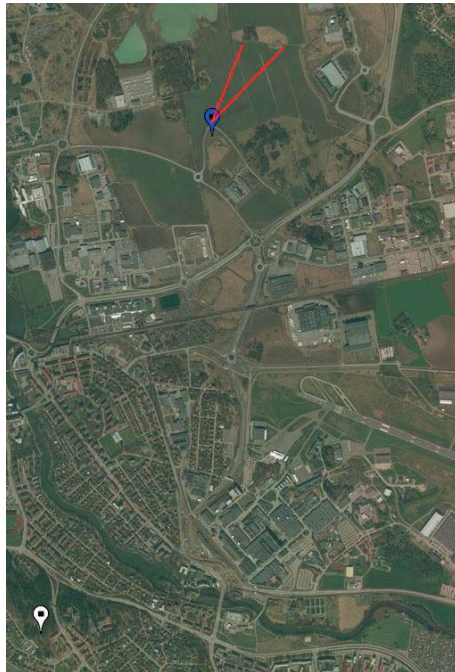

Figure 7.3: *Geometry during the UAV measurement. The white marker is the location of the transmitter, the blue marker is the location of the receiving antenna and the red lines are the approximate flightpath of the UAV.*

These measurements were conducted on a path that almost had a straight alignment between the transmitting antenna, the measuring site and the UAV, meaning that the UAV's almost full velocity should be detected. The bistatic range should also be close to the double of the true distance between the measuring site and the UAV, due to that the signal travels along the same path twice.
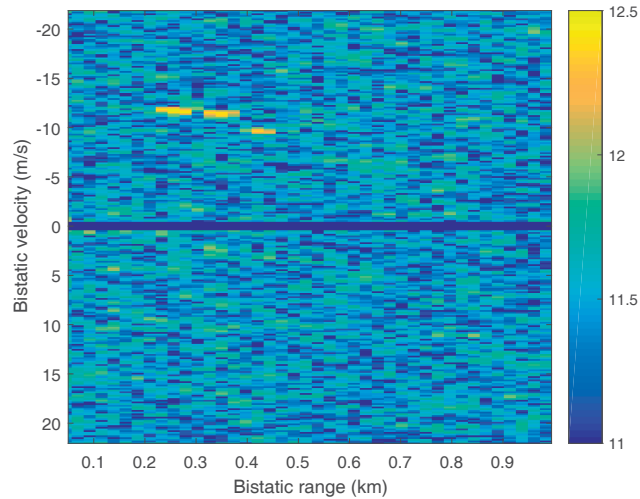
Figure 7.4: *The UAV approaching the surveillance antenna.*
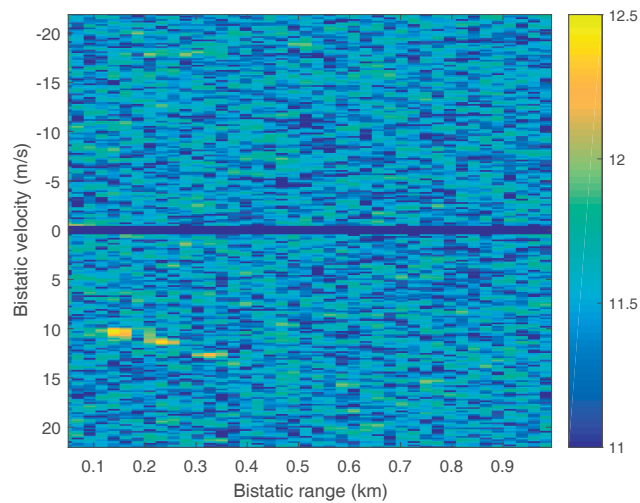
Figure 7.5: *The UAV receding from the surveillance antenna.*

The UAV used during the measurement was a custom built vessel with eight rotors made of carbon fiber. Including the battery it has a weight of 4.3 kg and a diameter of around 60-70 cm. During the measurement it flew with a top speed of approximately 15 m/s on a flight path of a couple of hundred meters, remotely controlled at a frequency of 2.4 GHz.

Figures 7.4 and 7.5 show two samples from the UAV measurement. In figure 7.4 the

UAV approaches the measuring site and in figure 7.5 it is receding. Both images consist of three consecutive measurements, each with an integration time of 1.84 seconds, that has been added in linear scale and are displayed in logarithmic scale. This relative long integration time is justified by the small target size and low velocities in order to increase the SNR of the UAV, even though the probability of range migration will be high.

The reference USRP had a signal gain of 10 dB while the surveillance USRP had a larger gain of 32 dB in order to account for the small target size.

7.4   Ground truth

The Radarcape along with the ADS-B receiving antenna were intended to be used as ground truth against measurements carried out against commercial aircrafts. As the result from the landing aircraft indicates, together with a number of previous measurements that did not detect any targets, this PBR system can not be shown to have an effective range beyond a bistatic distance of around 1.5 km. Furthermore, the measurement of the landing aircraft in the preceding section did for reasons unknown not communicate with the Radarcape the way it was intended. Learned from previous attempts, this flight among several others did not work with the Radarcape and can thus not be compared with the measured results. This phenomenon is suspected to depend on the coding that is used when sending the information between the aircraft and receiver.

The opportunity to obtain results for comparison with that of the Radarcape were consequently virtually non-existing due to the circumstances during this thesis, *i.e.* no close targets except the landing aircrafts.

In figure 7.6 the intended comparison between the Radarcape and an actual measurement is shown, which yielded no result due to the large distance. It was carried out from the roof at FOI, the black marker, and used the same transmitter as the other measurements, the red marker. The surveillance signals total path length would have been calculated from the bistatic range by adding the length of the baseline at a certain time during the measurement. This would then have been used to calculate the semi-major and semi-minor axis of the bistatic ellipse, which is the red ellipse in the figure. The ellipse is thus not constructed with values obtained by a real measurement, but is only there to show how the validation process would have been performed. Comparing the ellipse with the same time stamp on the obtained data from the Radarcape, the blue line, would then show an intersection between the ellipse and the flightpath. A successful measurement with an intersection where the time stamps would be equal would have validated the system.

Figure 7.6 as well as figure 7.1 and 7.3 were created in MATLAB using the webmap utility using coordinates obtained from Google Maps.
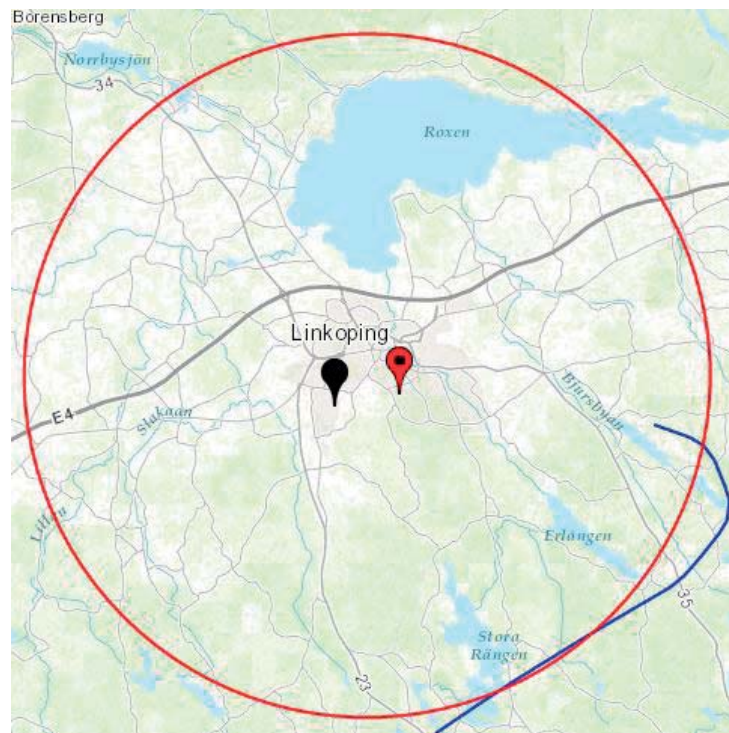
Figure 7.6: *Comparison between data collected by Radarcape and actual measurement. The red line is hypothetical, resembling an ellipse calculated from measured data and the blue line uses data from the Radarcape to show the target's actual flightpath.*

Chapter 8

Conclusions

The final chapter in this thesis accounts for the achievements of this project. Certain limitations of the PBR system will be mentioned as well as further improvements that can be investigated. Possible applications that can be realized based on the concepts and results of this thesis will also be discussed.

8.1 Achievements

For this thesis a functioning PBR system has been constructed by using general SDRs, ordinary TV-antennas and a commercial DVB-T antenna as a transmitter of opportunity. The system offers a high flexibility so that multiple SDRs can be easily integrated and tuned to different center frequencies in the range of 470-790 MHz.

In order to synchronize all devices an octoclock CDA-2990 was implemented in the system. This together with a signal generator in conjunction with a switch made it possible to make sure that the SDRs were aligned, enabling the devices to start their sampling simultaneously with insignificant phase shift between them.

Furthermore, an ADS-B receiver were incorporated in the system. This ought to be able to properly validate the accuracy of the system should results be obtained containing a target that properly sends information to the Radarcape. Due to the presumably short range of the system this proved to be unachievable under these circumstances.

Nevertheless, the results obtained with this system provides a proof of concept, yielding feasible bistatic ranges and bistatic velocities both for a large commercial aircraft as well as for a small sized UAV. Taking into account the wavelength at 474 MHz of 0.63 m, which was the center frequency being used, the detection of an UAV with a limited amount of reflecting material is the most significant result of this thesis. Since the UAV had a size on the same order of magnitude as the wavelength, these results could however be a consequence of the increase in SNR due to resonance. Although the tested distances were small, assuming that a stronger transmitted signal increases the effective detectable

range of such a small target as an UAV offers several possible applications for surveillance purposes.

8.2   System limitations and improvements

Several inconclusive live measurements on targets at large distances together with the obtained results in Chapter 7 indicates that the range of the system is relatively short. A reason for this could be due to not sufficiently high signal power at the DVB-T transmitter in Linköping that transmits at 2 kW, in comparison with *e.g.* the transmitter in Motala which has 50 kW or Nacka in Stockholm which has 150 kW. The transmitted power affects the range of any PBR system as shown in (2.6), as the received power is proportional to the inverse of the square of the distances from each antenna. Any increase of transmitted power is thus desirable to increase the range. Another reason could very well be that the targets that were not detected during measurements had too high altitude, being outside the beam of the transmitter since it was directed downwards.

For PBR systems in general the main drawback is the lack of control of the transmitter. Hence, each individual system has to be customized in order to effectively function with respect to possible limitations the transmitter may offer. In the case of this thesis the not sufficiently high transmitted power or the directivity of the transmitter presumably restricted the system to only successfully detect targets at a relatively short range. At a location such as Linköping, a PBR system would thus probably benefit more by using *e.g.* FM, GNSS or another commercial frequency band if it would allow the system to increase the range. This would however alter the properties of the constructed system, such as the resolution, but the results would suffer less from longer integration times due to the shorter bandwidths used [3].

As is shown by the characterization of the USRP N200, the choice of the center frequency give rise to different internally created spurs. These would most likely degrade the functionality of the system and will have to be removed in order to obtain a clean spectrum. Although, at some frequencies these were located inside the usable bandwidth, limiting the possible center frequencies that can be used flawlessly. It is possible that a more expensive and efficient SDR would allow the whole frequency span to be used without hindrance. This could also make the need to calibrate the devices obsolete since a more expensive device could very well make use of the same LO for two receiving channels.

The sampling frequency used during this work results in a large amount of data that needs to be transferred. The flexibility of the system, *i.e.* the number of USRPs that can be incorporated is thus limited by the performance of the Ethernet interface. For this work each USRP had its own LAN, although it would theoretically be possible to have two on the same network, there would be a low margin for error since the data transfer rate would be close to its limit. The amount of SDRs is thus limited to the amount of network interface cards that can be attained.

The results of this thesis were obtained by using relatively long integration times which leads to a high risk of range and Doppler migration. This was however needed in order to achieve the noticeable results as seen in Chapter 7. Other processing methods could improve the system, as well as achieve longer integration times without range and Doppler migration as in [10], where they utilize the Keystone transform for this purpose. Another

common approach is to use the envelope shift.

By measuring the background noise, where no targets are present and then subtracting this from target measurements, can potentially reduce the noise and increase the targets SNR. This method was tested but did for unknown reasons not work as intended and no further attempts were made to make this function properly. However, this method has the potential to increase the detectable range of the system by reducing the noise floor. Another possible method would be to decode the DVB-T signal to apply modifications and then recreate it to reduce the noise.

There also exist methods to achieve a finer spectrum, where one of the easiest to implement would be to use a cyclic correlation which would reduce the transient noise by avoiding sharp transitions between each correlation. Despite that this would be an easy way to improve the system this was not implemented due to more consideration taken to achieve any viable results.

Attempts could be made to be able to classify targets with the use of micro-Doppler signatures. These signatures arise from vibrations and motion of small moving parts on the target [11]. Knowing the characteristics of a certain vessel would allow the system to recognize what type of target that is detected.

In order to be able to extract more information from detected targets multiple receivers could be implemented, either collocated or separated by some distance. If all receivers detect the same target it would enable the system to determine the targets location, direction and also its true velocity.

Care could be taken to decrease the computational load of the system by reducing the amount of data that is processed. This can be achieved by either reducing the integration time or by lowering the sampling frequency. As stated previously, the long integration times used in this project were needed in order to achieve viable results. Although, with either a more powerful transmitter or possibly enhanced signal processing, it is possible that this duration could be reduced. The sampling frequency could be lowered to some degree but with an increased risk of mitigating the signal reconstruction. Should the load be reduced and powerful computational tools be utilized it would be possible to achieve real-time processing.

Although it was realized that the range was limited, either due to properties of the transmitter or by the signal processing, it should be noted that the system were comprised of generic components, not dedicated to be a part of a radar system. Further investigation could very well reveal a component as the bottleneck of the system.

8.3 Possible applications

The following applications show examples of when a PBR system could very well be used with an advantage over a conventional monostatic radar. These do however not represent possible applications for the system constructed for this thesis, but the results obtained and the conducted research indicate that they could be possible after further development.

As mentioned in the introduction of this thesis a PBR system have many inherent positive effects, many of which offer benefits for military applications. It is possible to arrange the system in a multistatic geometry, consisting of multiple spatially dispersed receivers and possibly multiple transmitters of opportunity, arranging the components in a grid. This

would *e.g.* allow for a border surveillance that is virtually invisible to potential aggressors with only the transmitters as detectable weak spots. The extended geometry could also allow for an extended radar horizon compared to a monostatic radar, increasing the detectability of low altitude targets. Due to the forward scattering phenomenon it would also be possible, at least for some geometries, to mitigate the effects of radar countermeasures such as stealth technologies. Recent research also shows the ability for PBR systems to detect high accelerating targets with promising results, such as missiles and rockets by including the acceleration in the ambiguity function [19]. However, depending on the conditions given by the circumstances, the performance of a monostatic radar would probably be hard to surpass for a PBR system, allowing instead a PBR system to complement the surveillance system yielding the aforementioned effects.

Due to the high mobility, small size and no need for an excessive power supply also allows for a PBR system to be deployed in an urban environment. This would increase the security during sport and political events, allowing for detection of malevolent UAV's. The ability to detect UAV's would also allow for the PBR system to be a cheap alternative for commercial airports.

Bibliography

[1] P. Bezoušek. V. Schejbal. Bistatic and Multistatic Radar Systems. Radioengineering, vol. 17, no. 3. September 2008.

[2] James W.A. Brown. FM Airborne Passive Radar. 2013. Ph.D. Thesis UCL, London, UK.

[3] Jonas Myhre Christiansen. DVB-T based Passive Bistatic Radar. 2010. Report FFI (Norvegian Defense Research Establishment), Kjeller, Norge.

[4] R.S.A Raja Abdullah. A. Ismail. Forward Scattering Radar: Current and Future Applications. International journal of engineering and technology, vol. 3, no. 1, pp.61-67. 2006.

[5] Armin W. Doerry. Earth Curvature and Atmospheric Refraction Effects on Radar Signal Propagation. January 2013. Sandia Report, Sandia National Laboratories.

[6] V.I Kostylev. Bistatic Radars. In M. Cherniakov (Ed.). *Bistatic Radar: Principles and Practice*. John Wiley & Sons, Ltd, 2007.

[7] Christian R. Berger et al. Signal Processing for Passive Radar Using OFDM Waveforms. January 2010. IEEE Journal on selected topics in signal processing.

[8] T. Martelli et al. Multi-Frequency Target Detection Techniques for DVB-T Based Passive Radar Sensors. Sensors 2016, 16, 1594.

[9] T. Pető et al. DVB-T Based Passive Radar. Radioelektronika, 2014 24th International Conference. IEEE. DOI: 10.1109/Radioelek.2014.6828433.

[10] T. Shan et al. Efficient Architecture and Hardware Implementation of Coherent Integration Processor for DVB-based Passive Bistatic Radar. IET Radar, Sonar & Navigation, Vol. 10 Issue 1, 1 2016. DOI: 10.1049/iet-rsn.2015.0006.

[11] V.C. Chen et al. Micro-doppler effect in radar: phenomenon, model, and simulation study. IEEE Transactions on Aerospace and Electronic Systems, Vol. 2 Issue: 1 Jan 2006. DOI: 10.1109/TAES.2006.1603402.

[12] FOI. About FOI, October 2016. `http://foi.se/en/foi/About-FOI/`.

[13] John W. Franklin. `www.cse.unt.edu/~rakl/john-proposal.ppt`. Accessed: March 8, 2017.

[14] Gerard Frawley. Embraer ERJ-190, March 2017. `http://www.airliners.net/aircraft-data/embraer-erj-170175190195/406`.

[15] Paul Howland. Bistatic range, October 2016. `https://en.wikipedia.org/wiki/File:BistaticRange.png#filelinks`.

[16] Analog Devices Inc. IQ-Imbalance, March 2017. `https://wiki.analog.com/resources/eval/user-guides/ad-fmcomms1-ebz/iq_correction`.

[17] Günter Köllner. Radarcape, March 2017. `http://www.modesbeast.com/`.

[18] T.C. Leong. Bistatic Radar System Analysis and Software Development. December 2003. Thesis, Naval Postgraduate School, Monterey, California.

[19] K. Borowiec M. Malanowski. Accelerating rocket detection using passive bistatic radar. Radar Symposium (IRS), 2016 17th International. IEEE. DOI: 10.1109/IRS.2016.7497376.

[20] James A. Melvin, William L. Scheer. *Principles of Modern Radar, Vol. II: Advanced Techniques*. SciTech Publishing, 2003.

[21] W. Aspray O. Blumtritt, H. Petzold. *Tracking the History of Radar*. The IEEE-Rutgers Center for the History of Electrical Engineering & The Deutsches Museum, 1994.

[22] R. Svitek S. Raman. DC Offsets in Direct-Conversion Receivers: Characterization and Implications. IEEE Microwave Magazine, Vol. 6 Issue 3 September 2005. DOI: 10.1109/MMW.2005.1511916.

[23] Ettus Research. About USRP Bandwidths and Sampling Rates, March 2017. `https://kb.ettus.com/About_USRP_Bandwidths_and_Sampling_Rates`.

[24] Ettus Research. SBX 400-4400 MHz Rx/Tx (40 MHz), March 2017. `https://www.ettus.com/product/details/SBX`.

[25] Ettus Research. USRP Hardware Driver and USRP Manual, March 2017. `https://files.ettus.com/manual/page_sync.html`.

[26] Mark A. Richards. *Fundamentals of Radar Signal Processing, Second Edition*. McGraw-Hill Professional, 2014.

[27] Rasim Akin Sevimli. Target Detection and Imaging on Passive Bistatic Radar Systems. 2014. M.S. Thesis, Bilkent University, Ankara, Turkey.

[28] M. Skolnik. *Radar Handbook 3rd ed.* McGraw-Hill Professional, 2008.

[29] ADS-B Technologies, October 2016. `http://ads-b.com`.

[30] Televes. Data sheet, March 2017. `http://www.televes.`
`com/sites/default/files/HTE/ht/01030490_004_`
`es-pt-fr-en-it-de-pl-ru.pdf`.

[31] USRP users mailing list. ADC resolution, March 2017. `http://lists.ettus.`
`com/pipermail/usrp-users_lists.ettus.com/2013-November/`
`007735.html`.

[32] Arend G. Westra. Radar versus Stealth Passive Radar and the Future of U.S. Military Power. Jfq: Joint force quarterly, 2009 4th quarter, issue 55, p136. September 2009.

Appendices

Appendix A

PBR Manual

1 - Config
2 - Test sync
3 - Calibration
4 - Collect an amount of samples
5 - Collect during an amount of time
6 - View log file
7 - Enter aircraft names, separate (AND END!) with space
8 - Clear log file and exit
9 - Exit

After starting the program, all devices and objects in the program are initiated. Also, the octoclock sets the time in each USRP. The number of USRPs are hard-coded to be 2, and thus the code has to be modified at some places in order to function with more devices. The location of these changes is self explanatory as relevant code is already used for each existing device.

Config sets the parameters for the USRPs such as center frequency and gain that is specified by the user, and prints relevant information to the display and log file.

Test sync only test that the devices are synced. All synchronization and time setting are done at start-up. This is only used to verify that a GPS signal has been received and that the communication between the devices are working.

Calibration runs a series of measurements during a time interval set by the user. Each measurement collects 1 million samples with a sample frequency of 25 MHz and saves the samples to a calibration file. The USRPs should be connected to the signal generator via the switch while running this program. Due to the nature of the sinusoidal, the 25 MHz sample rate is needed because only either the I or Q part of the signal can be used.

When running **Collect an amount of samples** the user specifies an amount of samples to be collected and saved to file. This has thus far only been used as a test to verify that everything is working accordingly, both when collecting and processing with Matlab.

Collect during an amount of time collects samples during a time specified by the user. This is the main collecting program and should be the one used for live measurements. The samples are saved to files that changes name for each measurement and the number of samples collected for each file is saved in another file in correct order. If the program is restarted, all files will be overwritten by the new ones. The sample rate is set to 12.5 MHz because it is assumed that both the I and Q part of the signal will be used during the signal processing. Also, when running this option, information about all flights observed by the ADS-B antenna are saved to a file.

View log file prints the log file to the terminal.

After all measurements have been done, use the **Enter aircraft names, separate (AND END!) with space** option to enter the names of all aircraft of interests, as observed on the Radarcape live 2D output. All data collected from the ADS-B antenna during the live measurements that corresponds to these names will be saved to separate text files. Each name is also saved as a list in another text file, which makes it easier to import the data with *e.g.* MATLAB. When entering, each name should be separated with space, and due to implementation difficulties there also has to be a space after the last name entered.

Clear log file and exit deletes the contents of the log file and closes the program.

Exit closes the program.

After or during the program is running the sample files can be processed with *e.g.* MATLAB.

LUND

UNIVERSITY